JOURNAL OF GEOPHYSICAL RESEARCH, VOL. 102, NO. A4, PAGES 7249–7265, APRIL 1, 1997

Simulations of the *F* region during the January 1993 10-day campaign

C.G. Fesen,[1] B.A. Emery,[2] M.J. Buonsanto,[3] Q.H. Zhou,[4] and M.P. Sulzer[4]

Abstract. The 10-day World Day campaign during January 20–30, 1993, provided an opportunity to test the current capability of the National Center for Atmospheric Research general circulation models and to conduct simple numerical experiments to investigate possible causes of day-to-day variability. Detailed data sets from the Arecibo and Millstone Hill incoherent scatter radars provided information on the middle- and low-latitude thermosphere and ionosphere during low solar activity which can be compared with model predictions. The theoretical model was used to examine the impact of varying two of the model inputs: the high-latitude energy and momentum sources and the semidiurnal tidal waves from the lower atmosphere. These exercises indicated that varying the high latitude inputs affect the simulations even to relatively low latitudes. The neutral winds in the models were responsive to the level of auroral activity and also to the magnitude of the waves from the lower atmosphere, particularly the neutral zonal winds. The simulated h_{max} were only affected at night by varying the model inputs. Use of the assimilative mapping of ionospheric electrodynamics (AMIE) technique is necessary to produce realistic quiet-time zonal ion drifts at low latitudes following local sunset. The ion and neutral temperatures proved nearly insensitive to the specifications of the auroral or the tidal inputs, particularly the temperatures at Arecibo. This is in contrast to the observations in which temperatures may vary by up to 100 K from day to day with more pronounced variability at night. In the models, only a large geomagnetic disturbance produced a perturbation in the temperatures but with magnitudes significantly smaller than those observed. The discrepancies may indicate an underestimate of the high-latitude Joule heating due to small-scale variability in magnetospheric electric fields, which would affect the neutral circulation and composition, and inadequate representation of the F region dynamo and conjugate effects in the models.

Introduction

The Earth's polar atmosphere is a region providing important energy and momentum sources for upper atmosphere structure and dynamics. Indeed, frictional Joule heating of the neutral atmosphere by ions driven by magnetospheric convection electric fields is crucial in determining the overall energy budget of the thermosphere [e.g., *Cole*, 1962, 1975; *Dickinson al.*, 1984], while the ion drag on the neutrals is one of the dominant forces driving the neutral motion [e.g., *Cole*, 1971a, b; *Fedder and Banks*, 1972; *Mayr and Harris*, 1978]. The high-latitude electric fields may penetrate to lower latitudes, particularly during geomagnetically disturbed periods, impacting the electrodynamics at regions far removed from the pole [*Richmond et al.*, 1992; *Richmond*, 1995]. The circulation induced by the high-latitude energy and momentum sources can induce and transport composition anomalies and redistribute chemical species [e.g., *Hays et al.*, 1973].

For these reasons, geomagnetic activity and its effects are frequently invoked to explain much of the observed day-to-day variability in thermospheric and ionospheric fields. Another likely source is waves excited in the lower atmosphere that penetrate into the thermosphere. The effects of tidal waves are well known [e.g., *Forbes*, 1982] and continue to be investigated along with the effects of planetary waves and short period gravity waves.

Current general circulation models incorporate self-consistent generation of electric fields by the neutral tidal winds [e.g., *Richmond et al.*, 1992] simulating the powerful coupling of the thermosphere/ionosphere

[1]W. B. Hanson Center for Space Sciences, University of Texas at Dallas, Richardson.

[2]High Altitude Observatory, National Center for Atmospheric Research, Boulder, Colorado.

[3]Haystack Observatory, Massachusetts Institute of Technology, Westford.

[4]Arecibo Observatory, National Astronomy and Ionosphere Center, Cornell University, Arecibo, Puerto Rico.

Copyright 1997 by the American Geophysical Union.

Paper number 96JA03312.
0148-0227/97/96JA-03312$09.00

system. These models generally utilize simplified statistical representations of the convection electric field and particle precipitation which define the location and width of the auroral oval and the amount of energy deposited in it. However, techniques developed by *Richmond and Kamide* [1988], *Richmond et al.* [1988], and *Emery et al.* [1996], derive time-varying prescriptions of the convection electric field and particle precipitation which frequently exhibit large differences from the statistical patterns, particularly during geomagnetically disturbed periods. This so-called assimilative mapping of ionospheric electrodynamics (AMIE) technique provides arguably the most realistic representation of the high-latitude energy and momentum sources. Both the AMIE technique and the National Center for Atmospheric Research (NCAR) thermospheric general circulation model are evolving rapidly, making it difficult to compare current simulations with those past. The most recent AMIE simulations are described by *Lu et al.* [1996] and *Emery et al.* [1996] which utilized an earlier version of the general circulation model, the thermosphere/ionosphere general circulation model [*Roble et al.*, 1988].

Use of the AMIE technique generally results in better representation of Joule heating events and ion drag momentum sources; these affect the generation and propagation of large scale gravity waves during geomagnetically disturbed conditions. *Buonsanto et al.* [this issue] present the first thermosphere/ionosphere/electrodynamic general circulation model (TIEGCM) simulations to incorporate the AMIE technique. These past modeling investigations incorporating AMIE have focused on the middle- and high-latitude thermosphere during predominantly highly disturbed periods.

The 10-day World Day campaign during January 20–30, 1993, provided an opportunity to test the current capability of the NCAR general circulation models and to conduct simple numerical experiments to investigate possible causes of day-to-day variability. The numerical experiments examined the impact of varying two of the model inputs: the high-latitude energy and momentum sources and the semidiurnal tidal waves from the lower atmosphere. Detailed data sets from the Arecibo and Millstone Hill incoherent scatter radars provided information on the middle- and low-latitude thermosphere and ionosphere which can be compared with model predictions. These results are among the first to evaluate the effects of the AMIE technique on TIEGCM simulations of low latitudes and during geomagnetically quiet periods.

Model Description

The model used is the NCAR TIEGCM [*Richmond et al.*, 1992] which self-consistently calculates electrodynamical interactions in the coupled thermosphere/ionosphere system. The nonlinear primitive equations for momentum, energy, continuity, hydrostatics, current density, and the equation of state are solved for the neutrals and the ions. Densities of the neutral and ion species are calculated along with the ion, electron, and neutral temperatures and the neutral winds and ion drifts. The model latitude and longitude resolution is 5° by 5°. The vertical dimension is nonuniform and is formulated in pressure levels with two grid points per scale height. Typically, the model solves for 25 pressure levels extending from about 97 to 300–500 km with the upper boundary determined by the solar activity level; for this period, the upper boundary was around 400 km. The O^+-O collision cross section used in the model runs included the Burnside factor of 1.7 [*Salah*, 1993].

The inputs required by the model are prescriptions of the solar and geomagnetic activity and the waves from the lower atmosphere that penetrate the thermosphere. The latter are represented by upward propagating tides and are incorporated as perturbations to the lower boundary as described by *Fesen et al.* [1991]. Contributions from the semidiurnal modes (2,2) through (2,6) plus the diurnal (1,1) mode are included [e.g., *Forbes et al.*, 1993]. The prescription of the semidiurnal tides at 100 km, i.e., at the model lower boundary, for January were taken from the model of *Forbes and Vial* [1989]. The daily and 81-day averaged solar 10.7-cm fluxes during the January 1993 period were obtained from the National Geophysical Data Center in Boulder, Colorado; time histories of the solar fluxes during the campaign period are shown in Figure 1. The F10.7 solar activity index ranged from 100 to 110, while the 81-day average was about 130.

Using these solar fluxes, two TIEGCM simulations of the January 1993 campaign were made to investigate the response of the model fields to varying high-latitude inputs. One utilized a statistical representation of the magnetospheric convection electric field and particle precipitation. The other used the AMIE technique [e.g., *Emery et al.*, 1996] to derive time-dependent representations of the auroral oval and the energetic particle fluxes from data obtained during the campaign period. These two runs are termed the "no-AMIE" and "AMIE" runs, respectively.

For the no-AMIE run, three inputs are required to specify the high-latitude processes: the cross-polar cap potential (CCP), the total hemispheric power (HP), and the By component of the interplanetary magnetic field. Occasionally, measurements of HP and By are available. However, during the January 1993 period, the Kp index was used to represent the CCP and HP as CCP= $29 + 11 \times Kp$ and HP= $-2.78 + 9.33 \times Kp$; these formulae are from P. H. Reiff (private communication, 1985) and *Maeda et al.* [1989], respectively. The HP values were then used to select the appropriate convection pattern from the empirical model of *Heelis et al.* [1982] and the auroral particle precipitation pattern based on the model of *Fuller-Rowell and Evans* [1987]. Identical patterns are assumed in the northern and southern hemispheres. Similarly, the CCP is identi-

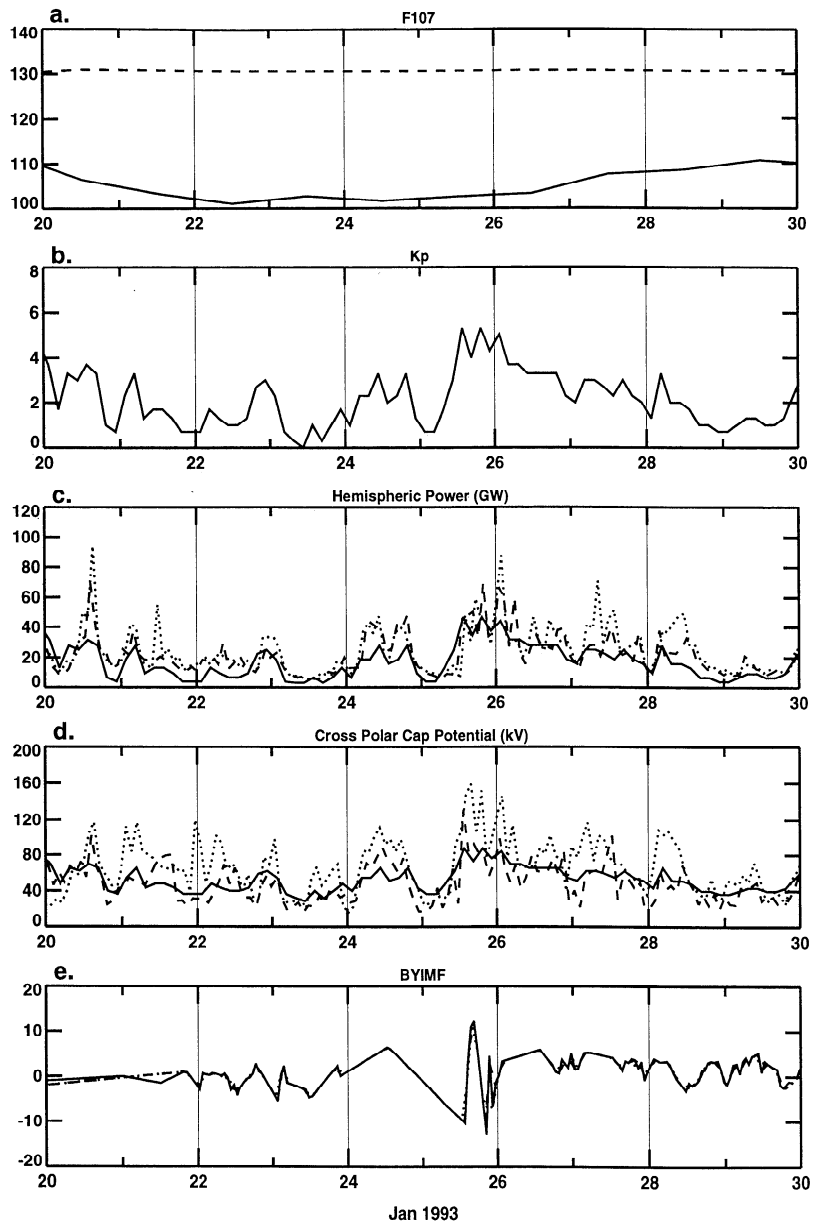

Figure 1. Geophysical conditions for the January 1993 10-day World Day campaign for the TIEGCM no-AMIE run: (a) daily (solid lines) and 81-day-averaged (dashed lines) solar fluxes; (b) Kp index; (c) total hemispheric power (gW); (d) cross-polar cap potential (kV); (e) IMF By component. Solid curves in (c), (d), and (e) are for TIEGCM; dotted curves and dashed curves show the AMIE inputs in the northern and southern hemispheres, respectively.

cal in both hemispheres, although the polar cap convection is asymmetric depending on the strength and sign of the interplanetary magnetic field (IMF) By component. The Kp indices and the CCPs, HPs, and By for the campaign period for the no-AMIE run are shown in Figure 1. The Kp index shows that the period was generally quiet although a disturbance occurred on January 25 when Kp was around 5. Accordingly, the CCP was typically $\leq$ 60 kV, while the HP was mainly $\leq$ 20 gW, and By was small except for a large perturbation on the 25th. Note that $Kp \sim 4$ late on January 19, just before the campaign started; the first day of the campaign followed a small geomagnetic disturbance.

Derivation of the high-latitude inputs using the AMIE technique for the January 1993 campaign is discussed in the work of *Buonsanto et al.* [this issue]; the salient point here is that the auroral input patterns were derived every 100 min. Figure 1 also shows the HP and CCP from the AMIE simulation. Since AMIE does not assume conjugacy between the northern and southern polar regions, the inputs derived for the northern and southern hemispheres differ and are shown in Figures 1c and 1d by the dotted and dashed curves, respectively. Hourly interpolated values of By from IMP 8 observations are shown in Figure 1e. It is obvious that the AMIE inputs are highly variable with large oscil-

lations present during the period, particularly in the northern hemisphere. The resulting perturbations to the high-latitude energy and momentum sources may generate gravity waves and traveling atmospheric disturbances (TADs) which may be manifested at low latitudes [*Buonsanto et al.*, this issue]. In contrast, the inputs used in the no-AMIE simulation are less variable and therefore less likely to spawn TADs.

A second exercise was done with the model to investigate whether the upward propagating tidal waves contribute to day-to-day variability. Three additional runs were made with the no-AMIE model to examine the sensitivity of the simulations to the semidiurnal tidal waves imposed at the model lower boundary. For this simple numerical experiment, runs were made for only one model day, January 20. In one simulation, the semidiurnal tidal amplitudes at the lower boundary were doubled over the values specified by *Forbes and Vial* [1989] for January. In the second simulation, the amplitudes were tripled. In the third simulation, no tidal forcing was imposed at the lower boundary. Similar exercises were not done with the diurnal 1,1 tide at the model lower boundary since this component does not penetrate beyond about 110–115 km altitude.

The magnification factors for the tidal amplitudes at the model lower boundary were chosen arbitrarily and purely in the spirit of a numerical experiment. Whether these magnification factors are justified is another question. Previous tidal studies with the NCAR models [e.g., *Fesen et al.*, 1993], which routinely use the *Forbes and Vial* [1989] model to represent the tides at the lower boundary, demonstrated that the model typically underestimates the tides in comparison with those observed. The cause of the weak model tides is not presently understood. One possibility is that the tides are dissipated too strongly in the model; this may occur if the ion drag is too strong. Later sections of this paper will show that this may indeed be the case. It should also be borne in mind that the Forbes and Vial tidal simulations represent averages which may not

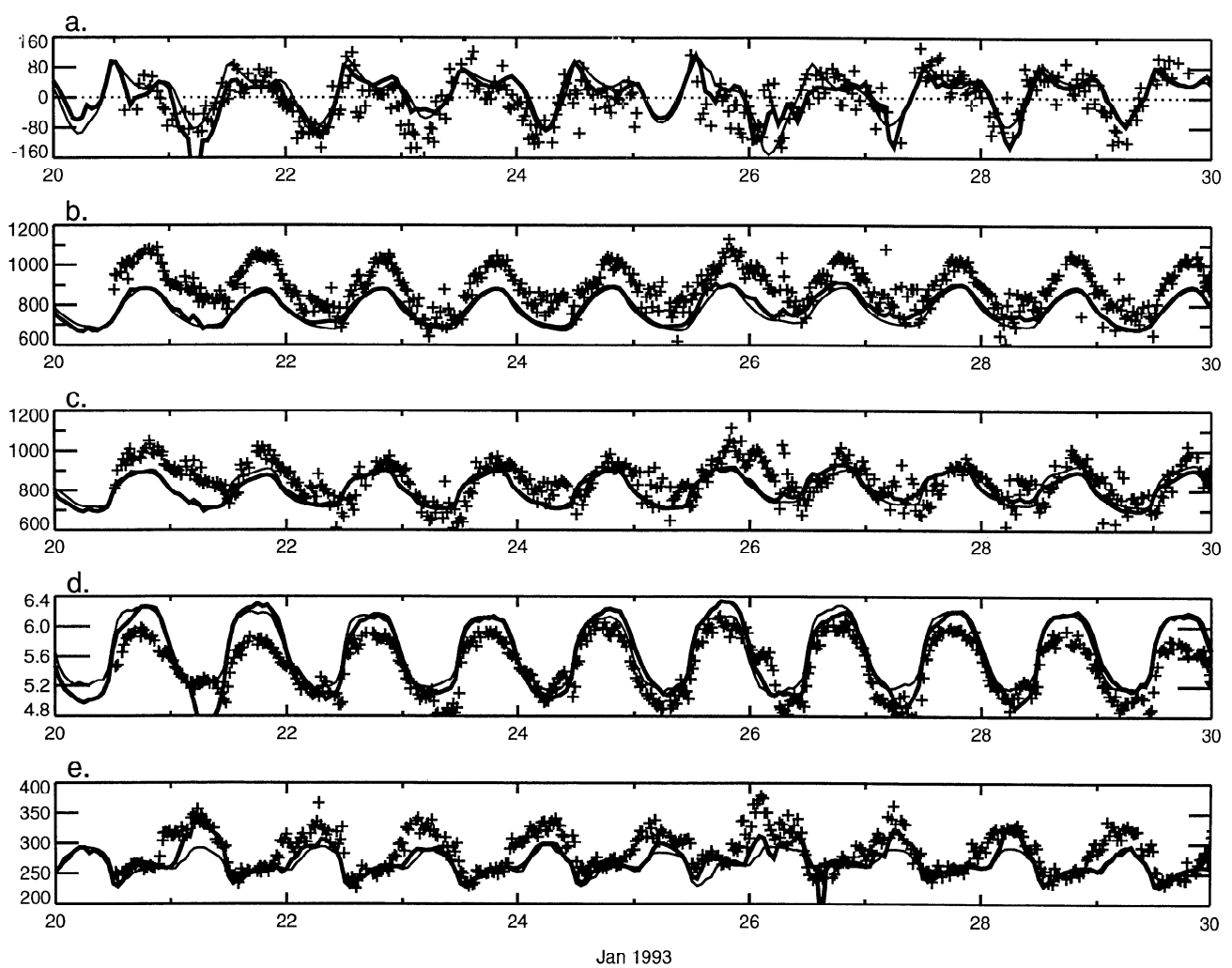

Figure 2. Simulations and observations of (a) the neutral meridional winds (meters per second) at 300 km; (b) the neutral temperatures (K) at 300 km; (c) the ion temperatures (K) at height h_{max}; (d) n_{max} (log 10 of the density cm^{-3}); and (e) h_{max} (kilometers) at Millstone Hill for the January 1993 10-day campaign. Heavy curves are the AMIE simulation, thin curves are the no-AMIE simulation. Observations are plotted as individual points.

be realistic at specific periods since substantial day-to-day variability is a hallmark of tidal observations [e.g., *Forbes,* 1984].

In the results presented below, zonal motions are positive to the east and meridional motions to the north. To focus this exercise, comparisons with data will be limited to the upper thermosphere and to the locations of Arecibo and Millstone Hill, representing a low-latitude site and a middle-latitude location, respectively. Note that in the following sections the neutral temperatures refer to a height of 300 km; the ion temperatures refer to the height h_{max} which varies diurnally from about 250 to 350 km.

Model Predictions for January 20–30, 1993

Millstone Hill

In this section comparisons are made between the observations and model at 300 km over Millstone Hill (42.6°N, 71.5°W). The observations are described by *Buonsanto et al.* [this issue] who also provide detailed comparisons of models and data for the geomagnetically disturbed period on January 24–26.

The neutral wind along the magnetic meridian, the neutral and ion temperatures, n_{max}, and h_{max} during January 20–30, 1993, are shown in Figure 2. The observed meridional winds exhibit a repeatable diurnal pattern, with poleward winds during the day, equatorward winds at night and speeds in the range ± 100 m/s. The models also exhibit a repeatable diurnal variation with speeds generally comparable to those observed. Sometimes the model winds vary more than those observed: For example, the models predict no nighttime surge on January 23 although one is seen in the data. Indeed, this feature is observed every night and is predicted every night except January 23. The AMIE simulated winds near 0000 UT on January 26 exhibit oscillations suggestive of a TAD, as discussed by *Buonsanto et al.* [this issue].

The neutral and ion temperatures are shown in Figures 2b and 2c, respectively. The observed neutral and ion temperatures, Tn and Ti, respectively, range between 700 and 1100 K. The models generally underestimate the temperatures by 100–200 K, particularly during the daytime. This may be due to an underestimate of high-latitude heating caused by small-scale fluctuations in the high-latitude electric fields as discussed by *Codrescu et al.* [1995] and *Buonsanto et al.* [this issue]. Biggest day-to-day differences in the data occur after geomagnetic disturbances when larger peak temperatures are observed. In contrast, little daily variability is predicted by the models.

The observed n_{max} (Figure 2d) show daytime peak densities ranging from 0.7 to 1.5 x 10^6 cm^{-3} with nighttime minima ~ 10^5 cm^{-3}. The models generally overestimate the densities, particularly during the daytime; as a result, the amplitude of the diurnal variation is larger in the models than in the data. The day-to-day variations in observations of n_{max} appear small; variability is more evident in h_{max} observations (Figure 2e), particularly at night. The AMIE model clearly better simulates this field, predicting significant day-to-day variability and successfully reproducing the high h_{max} on January 21 and 28. The oscillations predicted by AMIE near 0000 UT on January 26 result from oscillations in the meridional winds (see Figure 2a). Some of the variability in the neutral winds and consequently in h_{max} are in response to the gravity waves generated by high-latitude Joule heating events which are better represented in the AMIE simulation.

The disagreement in n_{max} between the models and the data may be due to discrepancies in the neutral densities, particularly the molecular densities. At F region heights, the electron density approximately equals the O^+ density. The O^+ is produced by photoionization of atomic oxygen and lost by reactions with N_2 and O_2. Thus n_{max} and h_{max} depend on the $O/(N_2 + O_2)$ ratio. Clearly, the production of O^+ is directly proportional to [O]. However, the role of N_2 and O_2 on the F region electron densities is more complicated: While these constituents destroy electrons through ion-molecule reactions, they also play a role in ion production through their influence on atmospheric optical depth.

The atomic oxygen and molecular oxygen and nitrogen densities from the empirical mass spectrometer/incoherent scatter (MSIS) model [*Hedin,* 1991] were computed for the period January 20–30 and compared with predictions from the two NCAR models. The results are shown in Figure 3 along with the ratio of atomic oxygen to molecular oxygen and nitrogen. Figure 3a shows the model atomic oxygen densities along with densities inferred from the Millstone Hill data near 400 km during the daytime. The MSIS densities are larger than those in the NCAR models by 50% or more. The data indicate a larger diurnal variation than that predicted by the models; they agree better with MSIS predictions at some times and with NCAR predictions at other times.

The molecular densities predicted by MSIS and the NCAR models are shown in Figures 3b and 3c; unfortunately no data exist for comparisons. The MSIS densities exceed the NCAR predictions by factors of 2 to 4 or more. Consequently, the $O/(O_2 + N_2)$ ratio, shown in Figure 3d, is very different for the models: For MSIS, the ratio is $\leq$ 10, while in the NCAR models it ranges from 15 to 40. Thus the overestimate of n_{max} by the NCAR models relative to observed n_{max} may indicate that the molecular densities in the NCAR models are too small, in agreement with *Emery et al.* [1996] and *Crowley et al.* [1996].

An increase in the molecular densities in the NCAR models may also improve the model representation of h_{max} for the following reason. As is well known [e.g., *Rishbeth,* 1986], the height of the peak tends to occur where chemical loss balances diffusive transport, i.e.,

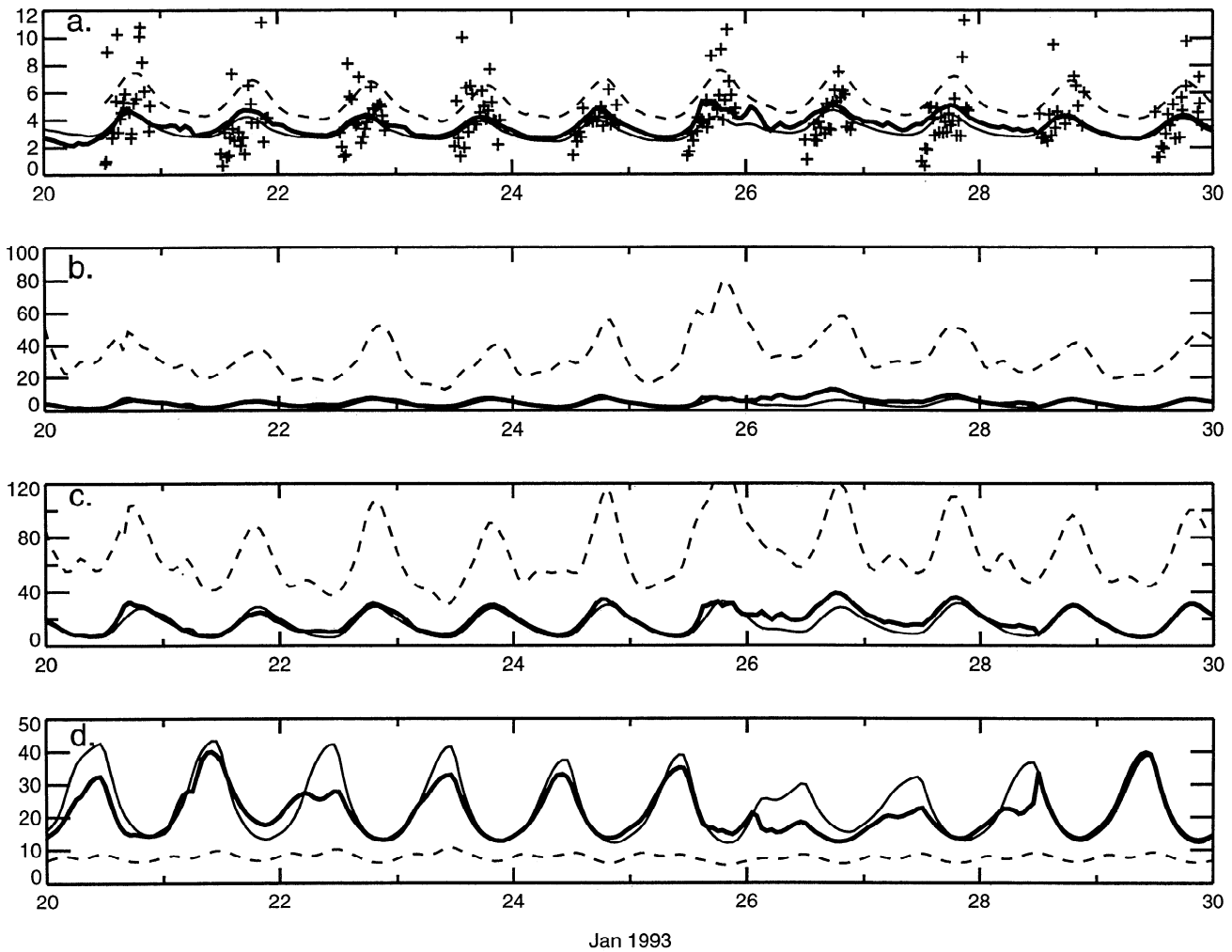

Figure 3. Simulations and observations of neutral densities at 400 km: (a) O (10^8 cm^{-3}); (b) O_2 (10^5 cm^{-3}); (c) N_2 (10^6 cm^{-3}); and (d) the ratio of $O/(O_2 + N_2)$. Broken curves show MSIS predictions; thick solid curves show AMIE simulations; and thin solid curves show no-AMIE simulations. Individual points are daytime densities inferred from observations at Millstone Hill.

where

$$\beta \sim \frac{D_a}{H_i^2} \tag{1}$$

where β is the chemical recombination rate of electrons with N_2 and O_2, H_i is the ionospheric scale height and D_a is the ambipolar diffusion coefficient. Both β and D_a depend on neutral density; β is directly proportional to molecular densities and decreases with height, while D_a is inversely proportional to atomic oxygen density and increases with height. If the neutral densities are increased in the NCAR model, β will decrease, D_a will increase, and the balance between the two processes will occur at higher altitudes, raising h_{max} in the model to improve its agreement with the data. As Figure 2c and 3d show, the differences between the calculated and observed h_{max} are particularly pronounced at night when the differences between the MSIS and TIEGCM densities maximize.

Arecibo

In this section comparisons are made between the modeled and observed ion drifts, ion temperatures, n_{max}, and h_{max} over Arecibo (18.3°N, 65°W). The ion drifts at 290 km are shown in Figures 4a and 4b; *ve* and *vu* are the drifts perpendicular to the geomagnetic field line in the eastward and in the northward/upward directions, respectively. The observed zonal ion drifts fall between ± 80 m/s; the northward/upward drifts range between ± 40 m/s with largest magnitudes near the terminators. Both components exhibit considerable scatter. Q. H. Zhou and M. P. Sulzer (Incoherent scatter radar observation of the *F* region ionosphere at Arecibo during January 1993, submitted to *Journal of Geophysical Research*, 1996) (hereinafter referred to as Zhou and Sulzer, submitted manuscript, 1996) found that the variability in the perpendicular eastward component is directly proportional to the

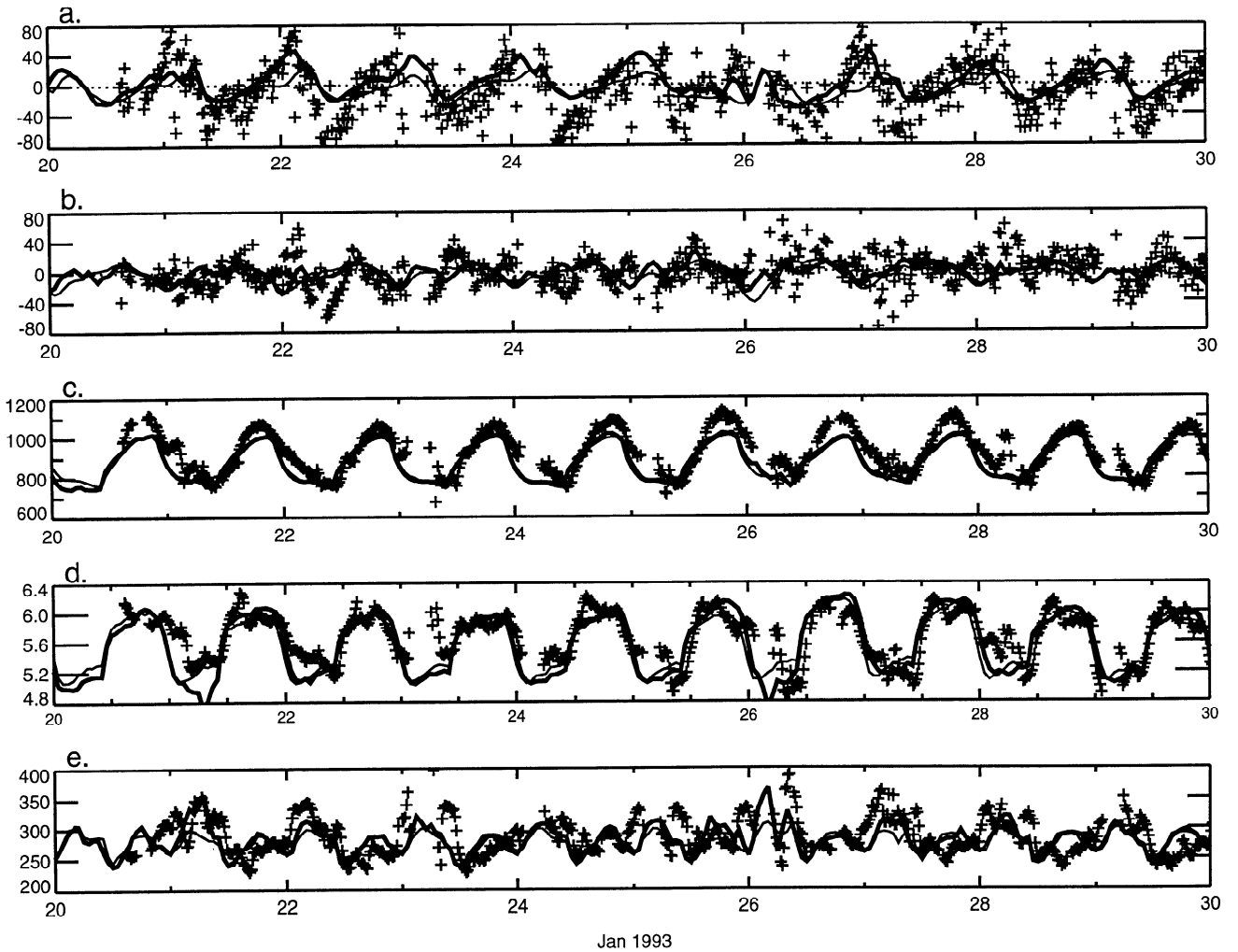

Figure 4. Simulations and observations of (a) the eastward ion drifts (meters per second) at 290 km; (b) the northward/upward ion drifts (meters per second) at 290 km; (c) the ion temperatures (K) at 290 km; (d) n_{max} (log 10 of the density cm^{-3}); and (e) h_{max} (kilometers) at Arecibo for the January 1993 10-day campaign. Heavy curves are the AMIE simulation, thin curves are the no-AMIE simulation. Observations are plotted as individual points.

magnitude of the drift. The variability in the perpendicular northward component is typically ≤ 20 m/s with minimal variability in the afternoon.

In general, the model drifts are in reasonable agreement with the data during the day (when *ve* and *vu* are eastward and northward, respectively). Main discrepancies appear at night, especially in *ve* for which the models fail to generate the observed peak westward drifts near 0900 UT; this will be discussed in the next section. The AMIE simulation is noticeably better than the no-AMIE run in representing the perpendicular eastward drifts around 0000 UT. The AMIE run also produces the greatest amount of day-to-day variability.

The ion temperatures at 290 km are shown in Figure 4c. The observed ion temperatures range between 700 and 1100 K with the variability ≤ 40 K (Zhou and Sulzer, submitted manuscript, 1996). The two models produce nearly identical results: The ion temperatures are typically underestimated, with maximum differences about 100 K at the daytime peak and little predicted day-to-day variability. This is consistent with the underestimate of the neutral temperatures at Millstone Hill. The ion temperatures are driven by heating due to collisions between ions and electrons and cooling by collisions between ions and neutrals. Both the electron and neutral temperatures at Millstone Hill were underestimated by the models [*Buonsanto et al.*, this issue] leading to an underestimate of Ti.

The observations of n_{max} and h_{max} are shown in Figure 4d and 4e along with the simulations. The observed n_{max} fall between 10^5 and 10^6 cm^{-3}; the day-to-day variation appears largely in the shape of the daytime peak and in the depth and shape of the nighttime valley. The model densities are in good overall agreement

with the data and with each other, although variability is more evident in the AMIE run. The observed h_{max} largely ranged from 250 to 350 km with significant day-to-day variations; the highest peak heights appeared within a day or two of geomagnetic disturbances. The modeled heights lie in the same range as those observed but exhibit smaller extrema. At night, the no-AMIE simulated heights are generally lower than the AMIE heights, presumably because of the weaker southward winds in the no-AMIE run consistent with less geomagnetic activity in that model. On most days the model h_{max} exhibit a clear semidiurnal variation, with contributions from the upward propagating tides [*Fesen,* 1996] as well as those generated in situ, as indicated by the sensitivity studies discussed later. The data do not appear to exhibit this behavior, perhaps because the phasing in the models is wrong. If such an oscillation exists it appears to be out of phase with the models at some times (e.g., near day 21 and just before day 29).

Averages and Daily Variability

The next figures illustrate the diurnal average variation of the observed and modeled fields at Arecibo and Millstone Hill during the quiet periods of the January 1993 campaign. Quiet periods were defined as those for which Kp was less than 4. As a result, about 15 hours of observations on January 25–26 were excluded from the averaging process. The observations for each day were binned into hourly averages to form the diurnal average. The degree of daily variability in the observations is also indicated; this was computed by calculating the standard deviations of the multiday averages and adding them to and subtracting them from the average at each local time. See *Buonsanto et al.* [this issue] for a description and discussion of the observations at Millstone Hill during the disturbed period of January 25–26 and comparisons with model predictions and Zhou and Sulzer (submitted manuscript, 1996) for further details on the observations and the averaging process at Arecibo.

Arecibo

The 10-day average perpendicular-east drifts *ve* at Arecibo are shown in Figure 5a; the thick solid line is the average derived from the observations; the thin solid lines on either side represent the daily variability, computed by adding and subtracting the standard deviations to and from the diurnal averages. The standard deviations are plotted separately in Figure 6 along with those from the models. The diurnally averaged drift is westward; peak westward drifts $\leq$ 50 m/s occur near 0400 LT and maximum eastward drifts of about 25 m/s near 2200 LT. The variability of the drifts, indicated by the thin solid lines, ranges from 20-40 m/s and, as mentioned earlier, is proportional to the magnitude of the drifts (Zhou and Sulzer, submitted manuscript, 1996) tending to be smaller during the daytime.

The broken curves show the diurnal average *ve* from the models. There is good agreement with the data during the daytime for both models; however, the evening eastward peak is only predicted by the AMIE run. Both models greatly underestimate the strong westward drift near sunrise. This may be due to inadequate representation in the model of the F region dynamo [*Rishbeth,* 1971] since the nighttime ion velocities depend on the F region polarization electric fields [*Behnke and Hagfors,* 1974]. In the model versions used here, the nighttime E region densities at the lower boundary are $\sim 10^4$ cm^{-3} which appear large enough to short out the F region dynamo and prevent it from developing at night [*Fesen et al.,* 1996]. A contributing factor may be the failure of the model to account properly for conditions at the ionospheric conjugate point; *Burnside et al.* [1983] attributed the large westward drifts near 0600 LT to the fact that Arecibo's conjugate point was sunlit. Since the model has a rigid upper boundary near 400 km, interhemispheric transport and its effects are not realistically represented in the model.

The observed perpendicular-northward drifts *vu* (Figure 5b) are generally $\leq$ 20 m/s. These averaged drifts from January 1993 differ from the December average for solar minimum at Arecibo [*Fejer,* 1993] which exhibit northward drifts of 25 m/s at 0400 and 1200 LT and southward drifts from 1400 to 2400 LT; the model drifts agree better with these latter averages. As Zhou and Sulzer (submitted manuscript, 1996) point out, *vu* observed during January 1993 appear more similar to *vu* during solar maximum conditions [*Fejer,* 1993] which may indicate a larger role is played by the solar fluxes averaged over several solar rotations (see Figure 1). The modeled drifts are small, in fair to good agreement with the observations; the biggest discrepancy occurs near 1800 LT where both models predict a southward surge, while the observed drifts remain near zero, perhaps further evidence for the need for more realistic modeling of the F region dynamo.

The average ion temperatures derived from observations (Figure 5c) exhibit a diurnal amplitude of about 250 K with a small midnight temperature maximum [e.g., *Harper,* 1973]. The two models overlie each other and typically underestimate the data up to 100 K for reasons discussed earlier.

The diurnal average n_{max} is shown in Figure 5d. The observations show a local maximum near 1000 LT followed by a broad peak persisting to about 1600 LT. In contrast, the models' daytime variation shows larger densities in the afternoon than in the forenoon with the evening decrease steeper and deeper than in the data. Since the modeled and observed daytime winds are in good agreement, the disagreement in n_{max} further supports the hypothesis that the neutral composition may not be well represented in the model. Electrodynamic

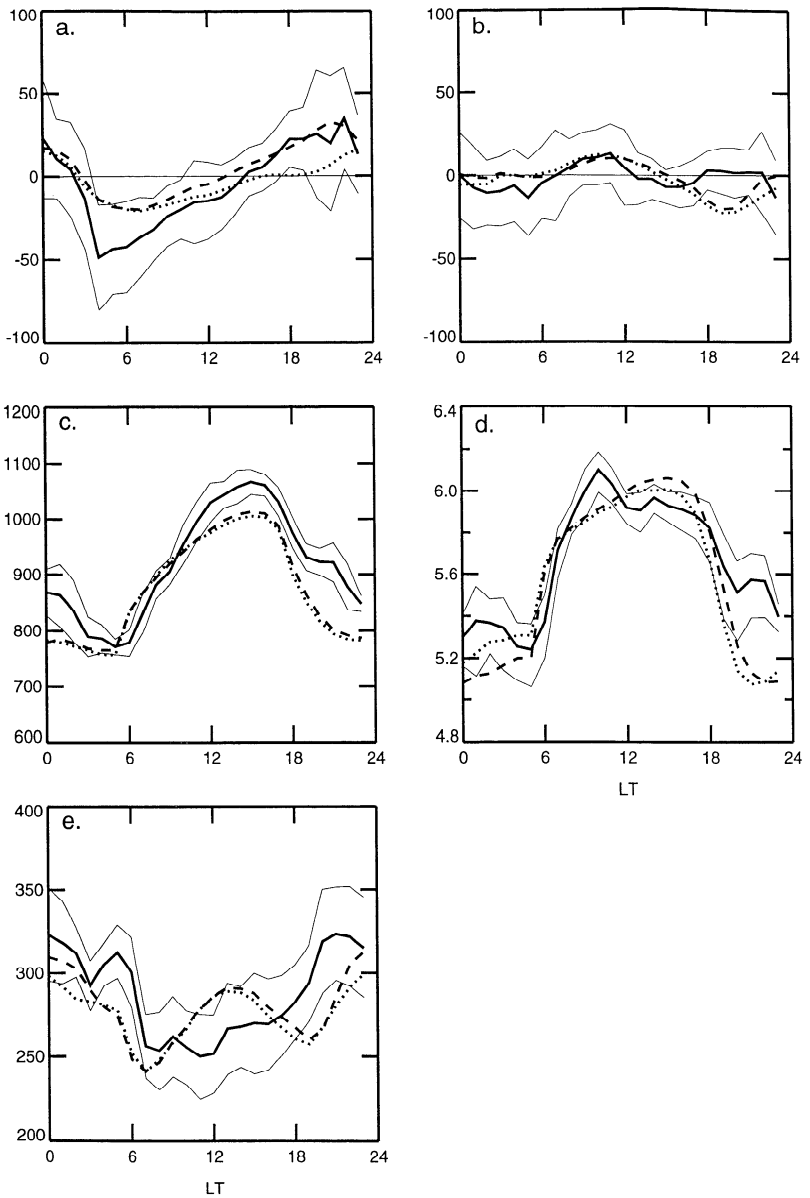

Figure 5. Diurnal averages from Arecibo during quiet periods of the January 1993 10-day campaign: (a) ion drift perpendicular to magnetic field in eastward direction (meters per second); (b) ion drift perpendicular to magnetic field in northward/upward direction (meters per second); (c) ion temperatures (K); (d) n_{max} (log 10 of the density cm^{-3}); and (e) h_{max} (kilometers). The thick solid curves are the observations; the dotted curves are the no-AMIE simulation and the dashed curves are the AMIE simulations. The thin solid curves are computed by adding and subtracting the standard deviations of the observations to and from the diurnal averaged observations; these represent the degree of variability of the observations. See text for details.

effects may also play a role, since the daytime n_{max} at low latitudes are dependent on dynamo electric fields which representation has not yet been carefully evaluated.

The observed and calculated diurnal average h_{max} are shown in Figure 5e. At night, the layer is observed to lie near 300 km on average; during the day, it descends as low as 250 km. The models predict a semidiurnal oscillation of h_{max} which appears out of phase with the data near sunset.

From inspection of Figure 5 as a whole, two noteworthy points can be made: The variances associated with the observations bracket the model predictions to a large degree, and the AMIE and no-AMIE simulations yield very similar results for the diurnally averaged fields.

The standard deviations are shown in Figure 6. For *ve*, the observations show variances ranging from about 15–40 m/s; the model variances are generally $\leq$ 10 m/s, although the AMIE simulated variances exhibit a local

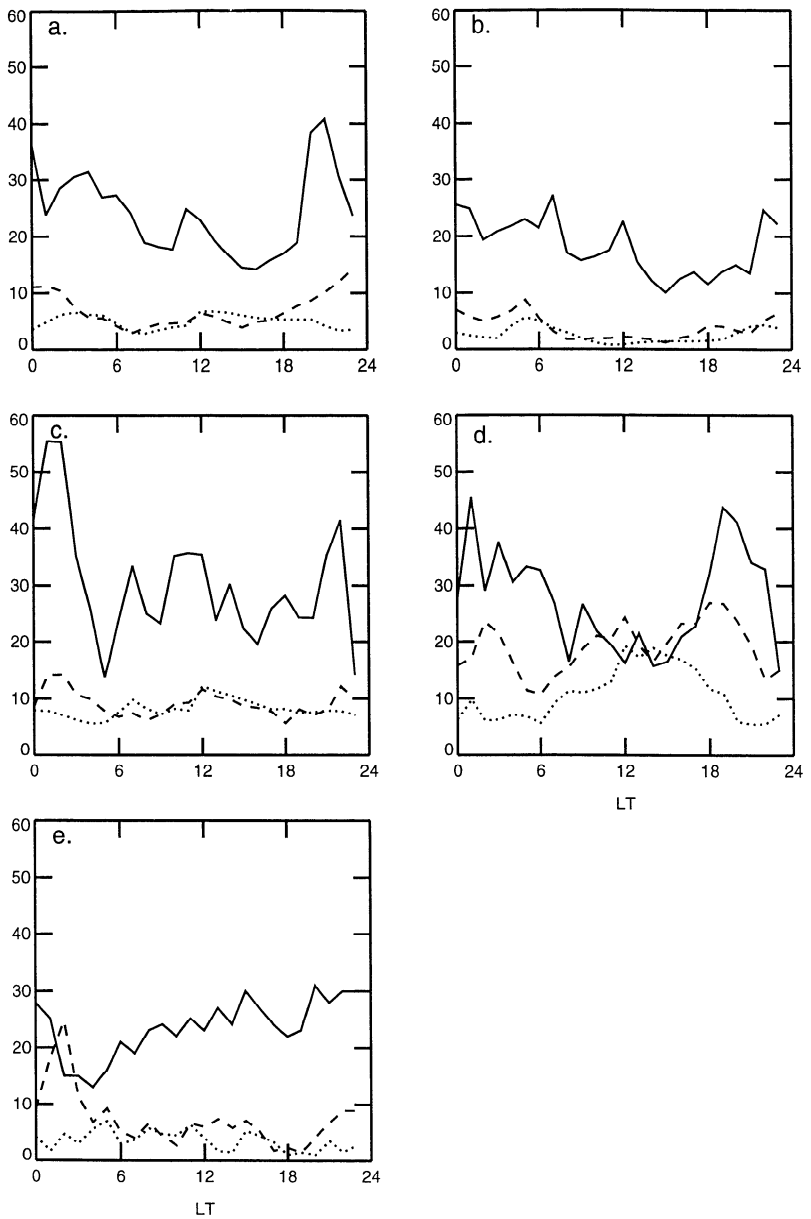

Figure 6. Standard deviations of the observations and simulations at Arecibo. Solid curve: data; dotted curves: no-AMIE; dashed curves: AMIE. The deviations for n_{max} are given as percentage differences from the diurnal average n_{max} at each local time. (a) ion drift perpendicular to magnetic field in eastward direction (meters per second); (b) ion drift perpendicular to magnetic field in northward/upward direction (meters per second); (c) ion temperatures (K); (d) n_{max} ; and (e) h_{max} (kilometers).

time dependence broadly similar to the observations. For *vu* (Figure 6b), the variability associated with the observations is about 20 m/s, while the models generally predict $\leq$ 5 m/s. For *Ti* (Figure 6c), the standard deviations calculated for the data average about 30 K; these include the fitting error, so the standard deviations due to geophysical factors may be smaller. The models predict standard deviations of only about 10 K. For n_{max}(Figure 6d), the observed variances are about 20–40% with smaller values during the day and larger values at night. For the models, the standard deviations in the no-AMIE run averages 10–15% with larger variances during the day. The AMIE simulation predicts larger variability, about 20%, with little local time dependence. Finally, for h_{max}, the standard deviations associated with the observations (Figure 6e) average about 20 km; in the models, the average is about 5 km, although the AMIE simulation exhibits large variability near midnight.

Millstone Hill

The diurnal averaged neutral and ion temperatures are shown in Figures 7a and 7*b*, respectively. The diurnal amplitudes are about 250 and 150 K, respectively.

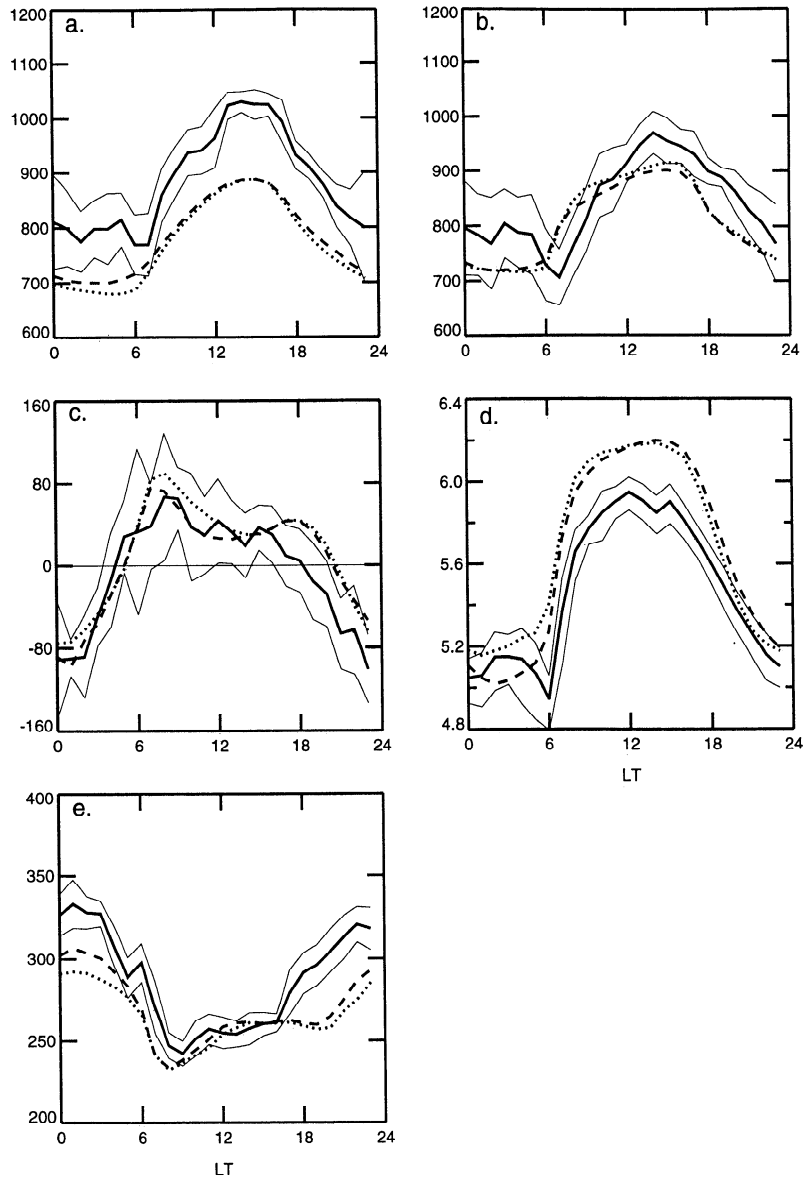

Figure 7. Diurnal averages from Millstone Hill during the quiet periods of the January 1993 10 day campaign: (a) neutral temperatures (K) at 300 km; (b) ion temperatures at 300 km (K); (c) magnetic northward neutral wind (meters per second) at 300 km ; (d) n_{max} (log 10 of the density cm^{-3}); and (e) h_{max} (kilometers).

As discussed earlier, the models underestimate the temperatures, more severely for the neutral temperatures than the ion temperatures, especially near midday.

The diurnal average meridional wind (Figure 7c) at Millstone Hill is observed to be northward during the day, peaking near 65 m/s at 0800 LT, and southward at night, peaking near 100 m/s at 2300 LT. The two models are in good agreement with the data from 0000 to 1600 LT. Near 1800 LT, the models exhibit a local maximum northward wind, while the observed winds steadily increase in the southward direction. The model results are suggestive of a semidiurnal tide which will be discussed further in the next section. Overall, the average winds derived from the observations are more southward-directed than the modeled winds, possibly indicating a higher level of geomagnetic activity than is represented in the models.

The diurnal average n_{max} derived from the observations is shown in Figure 7d along with the model predictions. The models typically overestimate n_{max}, especially during the daytime. As mentioned earlier, the differences may be due to deficiencies in modeling the composition. The observed and predicted h_{max} are shown in Figure 7e. The observations range from 250 km during the day to a maximum of 375 km near midnight. The model predictions are very similar to the observations during the day; at night, the model heights are lower than those observed by 50 km or so. This is

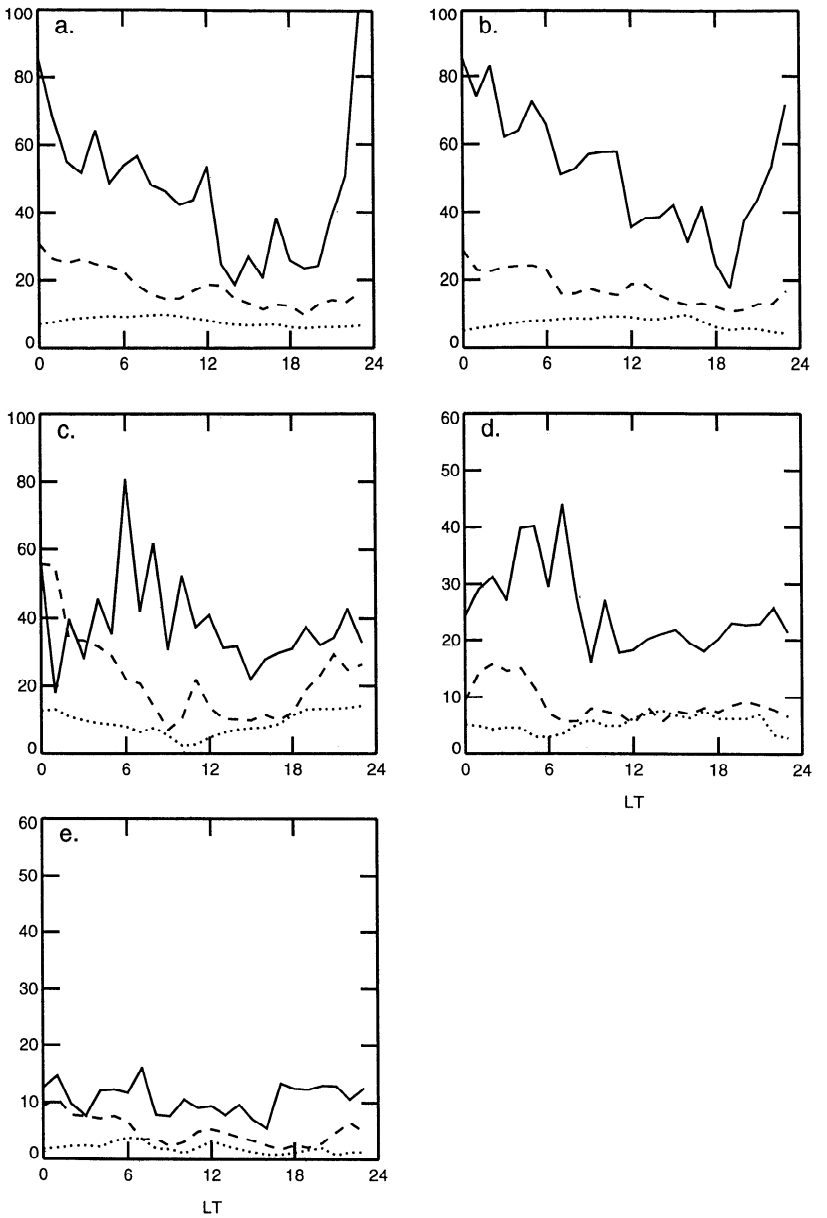

Figure 8. Standard deviations of the observations and simulations at Millstone Hill. Solid curve: data; dotted curves: no-AMIE; dashed curves: AMIE. The deviations for n_{max} are given as percentage differences from the diurnal average n_{max} at each local time. (a) neutral temperatures (K) at 300 km ; (b) ion temperatures at 300 km (K); (c) magnetic northward neutral wind (meters per second) at 300 km ; (d) n_{max}; and (e) h_{max} (kilometers).

due to the discrepancies in the meridional winds noted above; near 1800 LT, the models predict a northward wind which would lower the F layer, while the data show winds to the south which would raise the layer.

The standard deviations for Millstone Hill are shown in Figure 8. For the neutral and ion temperatures (Figures 8a and 8b), the observations have variances that are largest near midnight and smallest in the afternoon and near sunset, averaging about 40–50 K. The models predict smaller variances, of only 10 and 20 K in the no-AMIE and AMIE runs, respectively, with no significant local time dependence. For the magnetic meridional wind (Figure 8c), the data exhibit standard deviations typically of 30–50 m/s with larger variances at sunrise. The variances for the winds in the no-AMIE simulation are the order of 10 m/s; in the AMIE simulation, the variances vary more strongly with time and are appreciably larger at night, approaching the observations near midnight due to the influence of TADs and gravity waves. The variances in observations of n_{max} (Figure 8d) are roughly 20% during the day and 30% after midnight, while the models predict variances $\leq$ 10%. The standard deviations associated with h_{max} are small (Figure 8e): $\leq$ 10 km for both the models and the data although the AMIE simulation predicts somewhat larger variability than the no-AMIE run.

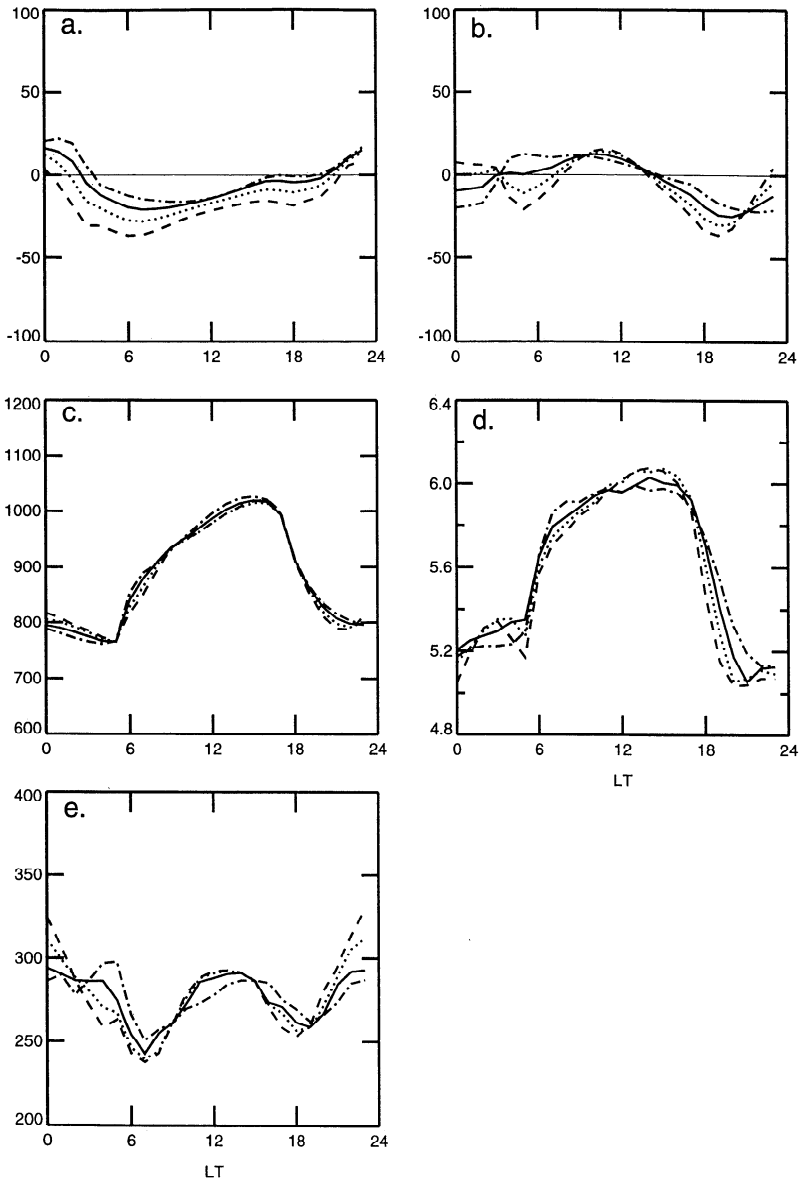

Figure 9. Simulations from the no-AMIE TIEGCM at the location of Arecibo for January 20, 1993, to illustrate sensitivity of the model fields to the tidal inputs at the lower boundary. (a) ion drift perpendicular to magnetic field, positive in the eastward direction (meters per second) at 290 km; (b) ion drift perpendicular to magnetic field, positive in the northward/upward direction (meters per second) at 290 km; (c) ion temperatures (K) at 290 km; (d) n_{max} (log 10 of the density cm^{-3}); and (e) h_{max} (kilometers). Solid lines are the simulations with the Forbes and Vial [1989] tidal amplitudes for January; dotted lines double the Forbes and Vial amplitudes; dashed lines triple the Forbes and Vial amplitudes. The dash-dot curve is the simulation with no tides at the model lower boundary. See text for details.

Variable Tidal Inputs at the Lower Boundary

The effects of changing the semidiurnal tides at the model lower boundary are next examined. Figure 9 shows the simulated fields at the location of Arecibo as the lower boundary tidal inputs are changed. The solid curves show the simulated field with the "standard" amplitudes and phases of the semidiurnal tides for January from *Forbes and Vial* [1989]. The dotted curves double the standard amplitudes, and the dashed curves triple the standard amplitudes. The dash-dot curves show the simulated fields for no tides imposed at the model lower boundary.

Inspection of Figure 9 shows that varying the tidal waves at the model lower boundary predominantly affects the nighttime simulations (i.e., from 1800–0600 LT). The perpendicular eastward ion drifts shift westward with increasing semidiurnal tidal amplitudes at the model lower boundary with biggest differences ~ 20 m/s. The perpendicular northward ion drifts may reverse in direction between 0000 and 0600 LT, changing

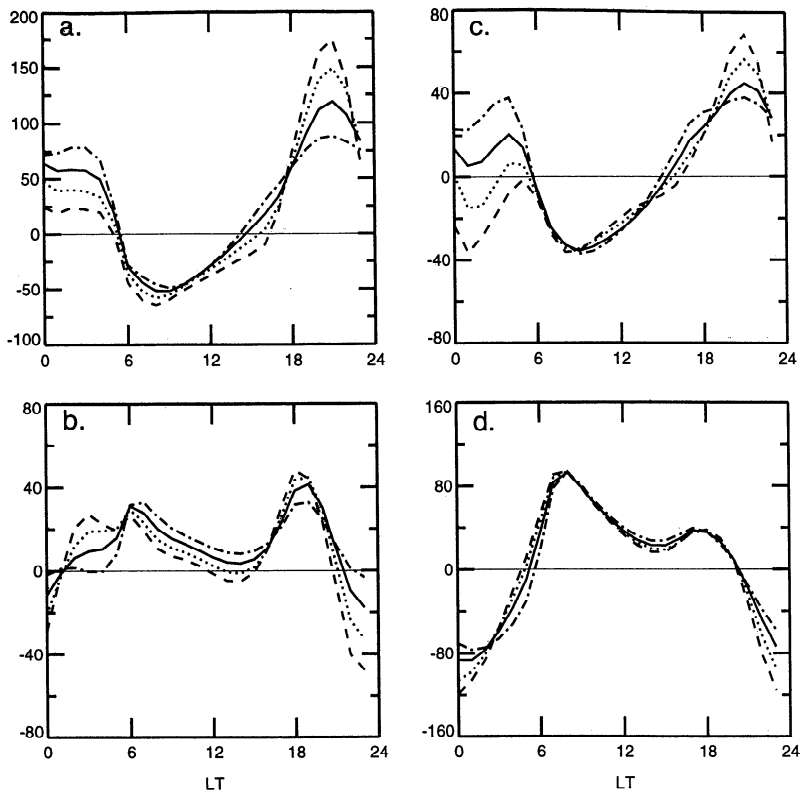

Figure 10. Simulations of the neutral horizontal winds at Arecibo and Millstone Hill for varying tidal inputs at the model lower boundary. (a) zonal neutral winds at Arecibo (meters per second), positive eastward, at 290 km; (b) meridional neutral wind at Arecibo (meters per second), positive northward, at 290 km; (c) zonal neutral winds at Millstone Hill (meters per second), positive eastward, at 300 km; and (d) meridional neutral winds at Millstone Hill (meters per second), positive northward, at 300 km. Solid curves: standard Forbes and Vial [1989] amplitudes for semidiurnal tides for January; dotted curves: Forbes and Vial amplitudes doubled; dashed curves: Forbes and Vial amplitudes tripled. The dash-dot curve is the simulation with no tides at the model lower boundary. See text for details.

by 20 m/s as the tidal amplitudes at the lower boundary increase. The southward surge at sunset also increases with the tidal amplitudes at the lower boundary. In these test cases, the phases of the tides at the lower boundary were not changed. A suitable adjustment of the amplitudes and phases at the model lower boundary could weaken or even reverse the modeled southward surge near sunset to produce better agreement with the data. Whether this exercise could provide a means to derive information on the tides at the model lower boundary remains to be explored. However, it appears promising, since the models predict that the tidal effects on the horizontal neutral winds may be dramatic, as demonstrated in Figure 10. At Arecibo (Figure 10a and 10b), differences of 40–50 m/s are predicted in the neutral winds at night.

The ion temperatures (Figure 9c) are not affected by the tidal inputs at the model lower boundary. However, because of the predicted tidal effects on the winds and drifts, differences appear in n_{max} and h_{max} for the three simulations, largely at night, as shown in Figures 9d and 9e, respectively. The differences in the tides at the model lower boundary can produce differences up to 25 km in the height of the F layer. However, the effects on n_{max} are generally small since there is no production of ionization at night and the transport acts only to redistribute the plasma.

At Millstone Hill the effects of the tides at the model lower boundary were generally small and not significant. There were a few exceptions, as demonstrated in Figure 10c, in which the model predicts large differences in the neutral zonal winds that result from varying the tides at the model lower boundary. Substantial differences occur between 2000 and 0600 LT; the winds at the later time even exhibit a shift in the predicted direction. Varying the tides at the model lower boundary caused the magnetic meridional wind (Figure 10d) near midnight to increase from -75 to -115 m/s. This lifts the F layer and decreases the peak densities near midnight, providing better agreement with the data at this time. The sensitivity runs imply that the tides are not the source of the local maximum in the model meridional winds near 1800 LT, leaving open the question of how to achieve better simulation of the observations.

Summary

Observations and simulations of the neutral and ionized atmosphere during the January 1993 10-day World Day campaign were used to evaluate the current capabilities of the NCAR general circulation model and the possible causes of day-to-day variability in the upper atmosphere. This was done by examining the model response to varying specifications of the high-latitude sources of energy and momentum and the semidiurnal tidal forcing at the model lower boundary. The high-latitude inputs were either specified from global data sets using the AMIE technique or by using empirical representations of the auroral oval, the no-AMIE technique.

In general, the models predicted the diurnal average variations during the quiet periods of the campaign reasonably well for the horizontal winds and drifts. The peak F layer densities were overestimated at Millstone Hill and underestimated at night at Arecibo. The F layer heights were modeled well at Millstone except from 1800-2400 LT; at Arecibo, the predictions were alternately higher and lower than those observed. The model temperatures were less than those observed which may indicate an underestimate of high-latitude heating due to small-scale variability in the electric fields. Such an increase in the heating would also affect the circulation and the ratio of atomic to molecular species which would improve the agreement with n_{max} and h_{max} at Millstone Hill.

Discrepancies between model and data tend to be larger at night. Electrodynamic effects are particularly strong in the time period from dusk to midnight [*Fejer*, 1993], implying that some of the model shortcomings may be due to inadequate development of the F region dynamo after sunset and inadequate accounting for effects of the conjugate ionosphere.

These exercises indicated that varying the high-latitude inputs may affect the simulations even to relatively low latitudes. In fact, for both simulations, the modeled n_{max} at Arecibo were more variable than those at Millstone Hill. At Millstone, better representation of the downward O^+ fluxes and conjugate effects in the models may be necessary to obtain improved agreement. Use of the AMIE technique is necessary to obtain realistic quiet time zonal ion drifts at Arecibo at night. In general, the variability in the model fields using the AMIE technique appeared more similar to the observations, although the magnitude of the variability was typically less than half as large as in the observations. The models successfully predicted more variability at night but at smaller levels than in the data.

The tidal waves from the lower atmosphere may contribute to the observed variability in the winds, drifts, and F layer heights at Arecibo, particularly at night, and may contribute to the westward surge in the ion drift that occurs near 0400 LT. Little effect is predicted on the temperatures. At Millstone Hill, the effects of the tides are smaller and confined to the midnight to dawn period. At both locations, midnight zonal neutral winds were especially responsive to the tidal variations.

The ion and neutral temperatures were relatively unaffected by variations in either the auroral or the tidal inputs. The temperatures at Arecibo were particularly insensitive to the changes in the model runs. This is in contrast to the observations in which the temperatures may vary up to 100 K from day to day with more pronounced variability at night. In the models, only a large geomagnetic disturbance produced a perturbation in the temperatures but with magnitudes significantly smaller than in the data.

Generating variability in the temperatures and the ion drifts will be very difficult, especially during the daytime when these model fields and the model neutral winds are essentially insensitive to changes in the current parameterizations of the high-latitude or low-altitude forcings. Since the model is a self-consistent physical representation of the upper atmosphere, there are only a few free parameters which can be adjusted in attempts to generate the observed variability. For the daytime discrepancies, one possibility is the solar forcing which is represented in the model by the 10.7–cm solar flux. This parameterization ignores the large variability at short wavelengths in the solar spectrum. Other possibilities are tidal waves and gravity waves. For the latter, of particular significance are those waves initiated by Joule heating events which may not be captured in the model and their subsequent interaction with other waves. Variations in n_{max} may also arise from variations in the high-altitude O^+ fluxes at night and from perturbations to the composition initiated by Joule heating. Better information on these parameters, along with the chemical composition, are required to achieve more accurate modeling of the thermosphere/ionosphere system.

Acknowledgments.
This research was supported by NASA grant NAGW 2656 and NSF grants ATM 94360 and ATM 94353 to Dartmouth College. One of the NSF grants was provided by the Coupling, Energetics, and Dynamics of Atmospheric Regions (CEDAR) initiative in the Aeronomy program of the NSF. The National Center for Atmospheric Research (NCAR) provided computing time and consulting assistance for this project; NCAR is also supported by the NSF. The Millstone Hill radar data were acquired and analyzed through the support of NSF cooperative agreements ATM-91-02445 and ATM-94-08609 to the Massachusetts Institute of Technology. Arecibo Observatory is the major facility of the National Astronomy and Ionosphere Center which is operated by Cornell University under a cooperative agreement with the NSF. The AMIE calculation owes thanks to many data providers. Electron precipitation measurements and estimates of the hemispheric power were provided by Fred Rich and Bill Denig of Phillips Lab for the DMSP satellites and by Dave Evans of the Space Environment Center for NOAA-12. The Goose Bay HF measurements were provided by Michael Ruohoniemi of the Applied Physics Laboratory to the CEDAR Data Base at NCAR which is also supported

by NSF. The Goose Bay HF radar is operated by the Applied Physics Laboratory of the Johns Hopkins University with support from NSF. EISCAT ion drifts were provided by T. S. Virdi of Aberystwyth, Wales. The EISCAT Scientific Association is supported by Centre National de la Recherche Scientifique of France, Suomen Akatemia of Finland, Max-Planck-Gesellschaft of Germany, Norges Almenvitenskapelige Forskningsrad of Norway, Naturvetenskapliga Forsknigsradet of Sweden, and the Science and Engineering Research Council of the United Kingdom. DMSP IDM and RPA drifts were provided by Marc Hairston of the University of Texas at Dallas. Ground magnetometer data were provided by Les Morris of the National Geophysical Data Center in Colorado, Eigil Friis-Christensen of the Meteorologisk Institut in Denmark, Mark Engebretson of Augsburg College in Minnesota, Terry Hughes of the National Research Council of Canada, David Milling of the University of York in the United Kingdom, Toby Clark of the British Geological Survey, and Carol Maclennan of AT&T Bell Laboratories in New Jersey.

The Editor thanks H. G. Mayr and another referee for their assistance in evaluating this paper.

References

Behnke, R. A., and T. Hagfors, Evidence for the existence of nighttime F region polarization fields at Arecibo, *Radio Sci., 9,* 211–216, 1974.

Buonsanto, M. J., M. Codrescu, B. A. Emery, C. G. Fesen, T. J. Fuller-Rowell, D. J. Melendez-Alvira, and D. P. Sipler, Comparison of models and measurements at Millstone Hill during the January 24–26, 1993 minor storm interval, *J. Geophys. Res.*, this issue.

Burnside, R. G., J. C. G. Walker, R. A. Behnke, and C. A. Gonzalez, Polarization electric fields in the nighttime *F* layer at Arecibo, *J. Geophys. Res., 88,* 6259–6266, 1983.

Codrescu, M. V., T. J. Fuller-Rowell, and J. C. Foster, On the importance of E-field variability for Joule heating in the high-latitude thermosphere, *Geophys. Res. Lett., 22,* 2393–2396, 1995.

Cole, K. D., Joule heating of the upper atmosphere, *Aust. J. Phys., 15,* 223–235, 1962.

Cole, K. D., Electrodynamic heating and movement of the thermosphere, *Planet. Space Sci., 19,* 59–75, 1971a.

Cole, K. D., Thermospheric winds induced by auroral electrojet heating, *Planet. Space Sci., 19,* 1010–1012, 1971b.

Cole, K. D., Energy deposition in the thermosphere caused by the solar wind, *J. Atmos. Terr. Phys., 37,* 939–949, 1975.

Crowley, G., C. G. Fesen, R. G. Roble, and A. D. Richmond, Verification of the TIEGCM for equinox, solar cycle minimum, *Eos Trans. AGU,* 77 (17), Spring Meet. Suppl., 1996.

Dickinson, R. E., E. C. Ridley, and R. G. Roble, Thermospheric general circulation with coupled dynamics and composition, *J. Atmos. Sci., 41,* 205–219, 1984.

Emery, B. A. et al., AMIE-TIGCM comparisons with global ionospheric and thermospheric observations during the GEM/SUNDIAL period of March 28-29, 1992, J. Geophys. Res., 101, 26, 681-26,696, 1996.

Fedder, J. A., and P. M. Banks, Convection electric fields and polar thermospheric winds, *J. Geophys. Res., 77,* 2328–2340, 1972.

Fejer, B. G., *F* region plasma drifts over Arecibo: Solar cycle, seasonal, and magnetic activity effects, *J. Geophys. Res., 98,* 13,645–13,652, 1993.

Fesen, C. G., R. G. Roble and E. C. Ridley, Thermospheric tides simulated by the NCAR TIGCM at equinox, *J. Geophys. Res., 98,* 7805–7820, 1993.

Fesen, C. G., Theoretical effects of tides and auroral activity on the low latitude ionosphere, *J. Atmos. Terr. Phys.,* in press, 1996.

Fesen, C. G., R. G. Roble, and E. C. Ridley, Thermospheric tides at equinox: Simulations with coupled composition and auroral forcings, 2, Semidiurnal component, *J. Geophys. Res., 96,* 3663–3677, 1991.

Fesen, C. G., G. Crowley, A. D. Richmond, R. G. Roble, B. G. Fejer, and L. Scherliess, Simulation of the pre-reversal enhancement in the low latitude vertical ion drift, *Eos Trans. AGU,* 77 (17), Spring Meet. Suppl., 202, 1996.

Forbes, J. M., Atmospheric tides, 2, The solar and lunar semidiurnal component, *J. Geophys. Res., 87,* 5222–5240, 1982.

Forbes, J. M., Middle atmosphere tides, *J. Atmos. Terr. Phys., 46,* 1049–1067, 1984.

Forbes, J. M., and F. Vial, Monthly simulations of the solar semidiurnal tide in the mesosphere and lower thermosphere, *J. Atmos. Terr. Phys., 51,* 649–661, 1989.

Forbes, J. M., R. G. Roble, and C. G. Fesen, Acceleration, heating, and compositional mixing of the thermosphere due to upward propagating tides, *J. Geophys. Res., 98,* 311–321, 1993.

Fuller-Rowell, T. J., and D. Evans, Height-integrated Pedersen and Hall conductivity patterns derived from the TIROS-NOASS satellite data, *J. Geophys. Res., 92,* 7606–7618, 1987.

Harper, R. M., Nighttime meridional neutral winds near 350 km at low to mid-latitudes, *J. Atmos. Terr. Phys., 35,* 2023–2034, 1973.

Hays, P. B., R. A. Jones, and M. H. Rees, Auroral heating and the composition of the neutral atmosphere, *Planet. Space Sci., 21,* 559–573, 1973.

Hedin, A. E., Extension of the MSIS thermosphere model into the middle and lower atmosphere, *J. Geophys. Res., 96,* 1159–1172, 1991.

Heelis, R. A., J. K. Lowell, and R. W. Spiro, A model of the high-latitude ionospheric convection pattern, *J. Geophys. Res., 87,* 6339–6345, 1982.

Lu, G., *et al.*, High-latitude ionospheric electrodynamics as determined by the AMIE procedure for the conjunctive SUNDIAL/ATLAS-1/GEM period of March 28-29, 1992, *J. Geophys. Res.*, in press, 1996.

Maeda, S., T. J. Fuller-Rowell, and D. S. Evans, Zonally averaged dynamical and compositional response of the thermosphere to auroral activity during Sept. 18-24, 1984, *J. Geophys. Res., 94,* 16,869–16,883, 1989.

Mayr, H. G., and I. Harris, Some characteristics of electric field momentum coupling with the neutral atmosphere, *J. Geophys. Res., 83,* 3327–3336, 1978.

Richmond, A. D., Modeling equatorial ionospheric electric fields, *J. Atmos. Terr. Phys., 57,* 1103–115, 1995.

Richmond, A. D., and Y. Kamide, Mapping electrodynamic features of the high-latitude ionosphere from localized observations: Technique, *J. Geophys. Res., 93,* 5741–5759, 1988.

Richmond, A. D., et al., Mapping electrodynamic features of the high-latitude ionosphere from localized observations: Combined incoherent scatter radar and magnetometer measurements for January 18–19, 1984, *J. Geophys. Res., 93,* 5760–5776, 1988.

Richmond, A. D., E. C. Ridley, and R. G. Roble, A thermosphere-ionosphere general circulation model with coupled electrodynamics, *Geophys. Res. Lett., 19,* 601–604, 1992.

Rishbeth, H., The F-layer dynamo, *Planet. Space Sci., 19,* 263–267, 1971.

Rishbeth, H., On the *F*2 layer continuity equation, *J. Atmos. Terr. Phys., 48,* 511–519, 1986.

Roble, R. G., E. C. Ridley, A. D. Richmond, and R. E. Dick-

inson, A coupled thermosphere/ionosphere general circulation model, *Geophys. Res. Lett., 15,* 1325–1328, 1988.

Salah, J. E., Interim standard for the ion-neutral atomic oxygen collision frequency, *Geophys. Res. Lett., 20,* 1543–1546, 1993.

M. J. Buonsanto, Haystack Observatory, Massachusetts Institute of Technology, Westford, MA 01886. (email: mjb@hyperion.haystack.edu)

B. A. Emery, High Altitude Observatory, National Center for Atmospheric Research, Boulder, CO 80307. (email: emery@ncar.ucar.edu)

C. G. Fesen, W. B. Hanson Center for Space Sciences, Physics Program, University of Texas at Dallas, POB 830688, MS FO22, Richardson, TX 75083-0688. (email: fesen@tides.utdallas.edu)

M. P. Sulzer and Q. H. Zhou, Arecibo Observatory, National Astronomy and Ionosphere Center, Cornell University, Arecibo, Puerto Rico 00613. (email: sulzer@naic.edu; zhou@naic.edu)

(Received May 22, 1996; revised September 25, 1996; accepted October 22, 1996.)